Electronic supplementary material for "Why is Amazonia a 'source' of biodiversity? Climate-mediated dispersal and synchronous speciation across the Andes in an avian group (Tityrinae)"

Lukas Musher[1*], Mateus Ferreira[2], Anya Auerbach[3], Jessica McKay[1], Joel Cracraft[1]

[1]Department of Ornithology, American Museum of Natural History, Central Park West @ 79th Street, New York, NY 10024
[2]Programa Pós-Graduação em Genética, Conservação e Biologia Evolutiva, INPA, Manaus, AM, Brasil
[3]Department of Ecology and Evolution, University of Chicago, 1101 E 57th Street, Chicago, IL 60637

Introduction:

Here we present our supplementary methods and results for genetic locus filtering, scoring of taxa for ancestral ecological analyses, bioinformatics, phylogenomic methods, macroevolutionary models, and additional discussion of biogeographic history and macroevolutionary patterns.

Supplementary Methods

Sequence capture of UCEs

We performed target-capture with the Tetrapods-UCE-2.5kv1 probe set (available at ultraconserved.org), which target 2386 UCEs. All individuals were previously extracted and many were previously sequenced for another study (Musher and Cracraft, 2018). For the remaining individuals, we sent extracts to Rapid Genomics (Gainesville, FL) for DNA shearing, library preparation, and UCE enrichment following the protocol detailed in Faircloth et al., (2012). Sequencing was performed on an Illumina HiSeq 2500.

Bioinformatic processing of UCEs

After sequencing, we cleaned data by removing low quality reads and trimming low quality base-pairs. We assembled reads using velvet (Zerbino and Birney, 2008) and matched these assembled contigs to the probes using prewritten python scripts from Phyluce (Faircloth et al., 2012). For one outgroup taxon, *Acanthisitta chloris*, we extracted UCE loci from assembled genomic read data available online (Jarvis et al., 2014). We matched the assembled contigs to UCE probes and incorporated the identified UCE markers into the sequence capture dataset explained above. Finally, we aligned orthologous loci for our final taxon set using MAFFT (Katoh and Standley, 2013). We chose to include all loci for which 95% of the individuals had sequence (henceforth, 95% complete dataset) for our molecular analyses.

Genetic locus filtering

We wrote custom scripts in R to quantify 1) the total number of parsimony informative sites, 2) the proportion of parsimony informative sites, and 3) two measures of clock-likeness for each marker. The latter were obtained by, first, using the chronopl rate-smoothing algorithm implemented in the R package "Ape" (Paradis et al., 2004) to estimate the optimal smoothing parameter (λ) using cross validation (compared multiples of 10 between 10^{-6} and 10^{2}), and then by performing likelihood ratio tests (clocklike to non-clocklike molecular models) at each locus

(see below). λ is a measure of clock-likeness, with higher values at a locus representing gene trees that have relatively even terminal branch lengths (i.e., gene tree shape is close to ultrametric), and lower values representing gene trees with more uneven terminal branch lengths.

Following Doyle et al. (2015) our intention was not to accept or reject a molecular clock at each locus, but rather to take loci that most closely fit with a clocklike model of molecular evolution (i.e., lower likelihood ratio). We used RAxML (Silvestro and Michalak, 2012) to build maximum likelihood (ML) gene trees at each locus using an automated shell script. We then imported these trees into R and calculated the likelihood of the gene tree, which represents a non-clocklike model estimate where branch lengths are calculated independently. We then calculated the likelihood of the gene tree given a clocklike model (i.e., an ultrametric model). To do this we used the Likelihood ratio, *LR*, which is given by two times the difference between log-likelihood of the clocklike model and log-likelihood of the non-clocklike model:

$$LR = 2 \bullet (lnL_{clocklike} - lnL_{nonclocklike})$$

In order to identify the markers that were most informative for divergence dating, we built a multivariate model in R that modeled LR as a function of the total variable sites, proportion of variable sites, and $\log_{10}(\lambda)$. As we are interested in divergence dating, clocklike markers are desirable, and those that deviate from clocklike tendencies were identified as outliers using Cook's distances (D). D values that were greater than three times the mean D were considered outliers, and removed from downstream analyses. Stated alternatively, loci that have exceptionally high or low values of LR, proportion of parsimony informative sites, or λ overinfluence the model result in high values for D and are considered outliers. Because Bayesian estimation of divergence times can be intractable for large molecular datasets, after removing outliers, we chose the 15 most clocklike (lowest LR) loci to use in divergence dating analysis. Our filtering regime is similar to that of Smith et al., (2018) in that we sort our markers by clock-like tendency, however we did not filter based on gene tree topology, and instead identify outlier loci by measuring the Cook's distance deviation from a linear model.

Phylogenomic analyses

In order to obtain a tree topology for divergence dating (see below), we concatenated all loci for the 95% complete dataset, and estimated the topology using RAxML (Silvestro and Michalak, 2012). We performed 20 Maximum Likelihood (ML) searches, under a GTRCAT model of substitution. The GTRCAT model approximates a GTR + Gamma model of sequence evolution (Stamatakis, 2006). We then performed bootstrapping using the autoMRE option, which halts bootstrapping after replicates converge. In our previous study on *Pachyramphus*, concatenated and species tree methods gave nearly identical topologies but species tree approaches experienced difficulty in placing individuals with relatively poor-quality sequence (Musher and Cracraft, 2018; see also Hosner et al., 2015). Because we included several individuals sequenced from museum study skins, which are likely to have poorer quality sequence than fresh tissue and can bias species tree results (e.g., Hosner et al., 2015; Musher and Cracraft, 2018), we chose not to use species tree approaches on this dataset, as the relationships in this group seem robust to methodological choices.

Reanalysis of the Claramunt and Cracraft (2015) dataset

The dataset from Claramunt and Cracraft (2015) used slow evolving nuclear genes (RAG1 and RAG2) and a fossil-calibrated dataset for family representatives across all Neornithes. We sampled RAG1 and RAG2 sequences available on GenBank (Tello et al., 2009)

for four additional taxa not included in the original study: *Schiffornis turdina, X. albinucha, P. polychopterus, and P. aglaiae*. We then incorporated these sequences into the original RAG dataset, keeping all priors and parameters identical, including fossil calibrations, and used BEAST v2.4.3 (Bouchaert et al., 2014) to generate a time tree. We ran the Markov Chain Monte Carlo (MCMC) with thinning of 1,000 for 1.9×10^8 generations. We assessed convergence using Tracer v1.6.0 (Rambaut et al., 2014), and then summarized the posterior distribution as a maximum clade credibility tree after a burnin of 25 percent.

MCMCTree Priors

We used the results from the Claramunt and Cracraft (2015) reanalysis to apply calibrations to our dataset of filtered UCE markers. We specifically obtained 95% credible intervals (CI) of node ages for crown Passeriformes, stem Tyranni, crown Tyrannides-Furnariides, crown Tyrannides, and crown Tityridae (taxonomic names *sensu* [35]). The locus substitution rate is defined by a gamma prior for mean substitution rates, $\Gamma(\alpha,\beta)$, where rate mean is equal to α/β and rate variance is equal to α/β^2. We applied a prior distribution of $\Gamma(2,200000)$, which defines a mean rate of 10^{-5} substitutions MY^{-1} assuming a one-year generation time. For the birth-death model, we applied uniform priors for birth and death rates of one, and sampling of 0.90. We then ran the MCMC for 1.5×10^6 generations following a burnin of 5×10^5 generations. We assessed convergence using Tracer v1.6.0 (Rambaut et al., 2014).

Ancestral ecological modeling and biogeographic inference

We quantified the amount of *in situ* speciation, lineage emigration, and lineage immigration for each biogeographic area in our Dispersal Extinction Cladogenesis (DEC) model – Amazonia, Atlantic Forest, Andes, arid diagonal, lowlands west of the Andes, and Central America. To do this, we defined total *in situ* speciation for each area as the total number of parent nodes whose maximum likelihood (ML) state contained at least one matching area in the maximum likelihood state of both of its daughter nodes. For example, if a node's maximum likelihood state was Amazonia, and both of its daughter nodes also contained Amazonia in their ML states, we considered this a single *in situ* speciation event for Amazonia. We defined total lineages emigrating from a given area as the total number of novel ML area states at daughter nodes stemming from all parent nodes whose ML state was the area of interest. For example, if Amazonia is the state of the parent node and one of its daughters contained an area other than Amazonia, we counted this as a single emigration event for Amazonia. And finally, we defined total immigration for each area as the number of daughter nodes whose parent node did not contain at least one of the same areas. For example, if a given daughter node contained Amazonia, but its parent node did not, we considered this a single immigration event for Amazonia.

For habitat affinity, we coded each species based on the its habitat codes found in Parker et al. (1996), and additional information where available (Fitzpatrick et al., 2004). Species found in F1 (Tropical lowland evergreen forest) or F4 (Montane evergreen forest) were coded as having an affinity for forest interior, while those found in other habitats, including F1E (edge) or F4E, were coded as having an affinity for semi-open habitat (this includes semi-open forests such as flooded, seasonally dry, white sands, and gallery). Taxa that use both types of habitat were coded as polymorphic. We constructed a model in RevBayes (Hohna et al., 2016) that allowed for equal probabilities of state addition and loss in habitat preference by employing a DEC model (Ree and Smith, 2008) that is implemented within the RevBayes language. We

chose a DEC model, designed for biogeographic analysis, rather than a discrete character evolution model because habitat is spatially distributed, and transitions occur in the same ways that dispersal into novel regions occurs – as a time-dependent process. Still, fitting a DEC biogeographic model, is akin to fitting a MK model of discrete character evolution. We put an exponential prior with mean of one state change per 20my per lineage. We ran the MCMC for 10,000 generations and summarized posterior probabilities of each ancestral state after a burnin of 25 percent. Scripts are available at https://github.com/lukemusher/Tityrinae_biogeography.

Macroevolutionary rates

To estimate diversification rates through time and among lineages, and to identify potential speciation or extinction rate shifts, we used both Bayesian Analysis of Macroevolutionary Mixtures (BAMM; Rabosky et al., 2014) and TESS (Hohna et al., 2015). TESS uses a reversible-jump MCMC (rjMCMC) algorithm to estimate the timing of rate shifts in speciation and extinction under an episodic birth-death process. We assumed 85% complete taxon sampling for the subfamily, expected number of rate changes of three (boundaries between epochs since Miocene), and zero mass extinctions. We estimated empirical hyperpriors for speciation and extinction. We ran the TESS analysis for 10^6 generations and assessed convergence in parameter estimates using Tracer v1.6.0 (Rambaut et al., 2014). BAMM also uses an rjMCMC to quantify diversification rate heterogeneity along a phylogeny, and we ran this analysis for 5 x 10^7 generations with thinning of 10^5 and a burn-in of ten percent. We optimized priors using the "setBAMMpriors" function implemented in the R package BAMMtools (Rabosky et al., 2014).

To test for diversity-dependent diversification, we also applied a model-fitting approach implemented in the R package, DDD (Etienne et al., 2012). We fit six models, four of which explicitly incorporate a parameter for carrying capacity (K): (1) birth-death constant rates without carrying capacity, (2) linear dependence of speciation rate on K without extinction, (3) linear dependence of speciation rate on K with extinction, (4) exponential dependence of speciation rate on K with extinction, (5) linear dependence of extinction rate on K, and (6) exponential dependence of extinction rate on K.

We then used the results of the TESS analysis to quantify the effect of palaeotemperature on net-diversification rate (speciation rate – extinction rate). We first divided the posterior net-diversification rates from TESS into 50 evenly-spaced intervals between the basal split and tips, and quantified mean posterior net-diversification rate for each interval in TESS. Then, using palaeotemperature data available in RPANDA (Morlon et al., 2016; Condamine et al., 2013), we quantified the relationship between temperature and net-diversification. To obtain temperature values for each interval, we took the mean of all temperature measurements within each time interval. We then evaluated their correlation using linear regression and compared three generalized linear models where net-diversification is either dependent on time, temperature, or interactive effects of both time and temperature.

Finally, as a more sophisticated test of environmentally-driven diversification we applied one additional model selection implemented in RPANDA (Morlon et al., 2016; Condamine et al., 2013), which explicitly models speciation and extinction rates and optimizes parameters. We fit ten models to our divergence time results from MCMCTree. We specifically fit (1) pure birth constant rate, (2) birth-death constant rates, (3) speciation varies exponentially with time and no extinction, (4) speciation varies exponentially with time and constant extinction, (5) extinction varies exponentially with time and constant speciation, (6) speciation and extinction vary

exponentially with time, (7) speciation varies exponentially with temperature and no extinction, (8) speciation varies exponentially with temperature and constant extinction, (9) extinction varies exponentially with temperature and constant speciation, and (10) speciation and extinction vary exponentially with temperature. To evaluate the effect of using stem or crown ages, we also employed this model selection twice, once conditioning each model on stem ages and once on crown ages.

For all model selection sets we compared likelihoods of each model and chose the model with the lowest corrected Akaike Information Criterion (AICc). Because in some cases multiple models differ only slightly in AICc, the relative fit of each model was assessed using AICc weights (AICω), which allow a more intuitive interpretation of the fit of each model relative to other models. AICω represents the conditional probability for each model. All scripts are available at https://github.com/lukemusher/Tityrinae_biogeography.

Supplementary Results

Data filtering

Our 95% complete UCE dataset contained 1,160 loci with a total of 825,445 bps. Using this concatenated alignment, RAxML recovered a topology identical to our previous study (Musher and Cracraft, 2018), except for the position of *Pachyramphus minor,* which was recovered with weak support (ML bootstrap = 55). We constrained the position of *P. minor* for divergence dating based on the more robust relationship recovered in our previous study (Musher and Cracraft, 2018). Because UCE datasets may contain aberrant loci that can cause problems for downstream analyses, we quantified informativeness and clock-likeness of each locus via two measures, λ and LR, and explored their relationship in addition to their relationship with locus informativeness (total number and proportion of informative sites)(Figure S1).

The number of informative sites per locus ranged from 4 to 273 (mean ± standard deviation = 99.22 ± 46.45), the proportion of informative sites per locus ranged from 0.0053–0.39 (mean = 0.14 ± 0.063), and the LR for each locus ranged from 2007.04–25800.57 (mean = 7360.096 ± 3608.302). Locus informativeness was correlated with both clocklike measures, but informativeness predicted significantly more of the variance for LR than for λ (total informative sites with $\log_{10}\lambda$: Adj. $R^2 = 0.05708$, F= 71.16, p = 0.0; Proportion informative sites with $\log_{10}\lambda$: Adj. $R^2 = 0.05731$, F= 71.46, p = 0.0; Total informative sites with LR: Adj. $R^2 = 0.1555$, F= 214.4, p = 0.0; Proportion informative sites with LR: Adj. $R^2 = 0.1812$, F= 257.5, p = 0.0). LR and $\log_{10}\lambda$ were also weakly correlated (Adj. $R^2 = 0.02058$, F= 25.35, p = 0.0).

Our glm that modeled LR as a function of informativeness and λ did not find λ to be a significant predictor in the model (p=0.073) but removing lambda did not improve the model's fit to the data (with λ AIC = 22054, without λ AIC = 22055). Our filtering protocol identified 83 outlier loci, which were primarily either loci that were very un-clocklike (high LR) given their informativeness, or very uninformative given their low LR (relatively few informative sites). Removing these loci from the dataset improved the relationship between locus informativeness and clock-likeness (Total informative sites with LR: Adj. $R^2 = 0.1791$, F= 235.8, p = 0.0; Proportion informative sites with LR: Adj. $R^2 = 0.2105$, F= 287.8, p = 0.0; Figure S1), and significantly improved the quality of the model fit (AIC = 15,507). Figure S2 shows 25 randomly-chosen examples of gene trees of loci that were identified as outlier loci (Figure S2A) and the 15 markers used in our divergence dating analysis (Figure S2B). Loci identified as outliers tended to have high values for LR with relatively low informativeness and were aberrant

in shape (mix of relatively long and relatively short branch lengths across the tree). After removing outlier loci, our 15 lowest LR UCEs (Figure S2B) ranged in LR from 2475 to 2909.

Time calibrated phylogeny

We reconstructed a time-calibrated phylogeny using the Claramunt and Cracraft (2015) dataset and recovered a timeframe of diversification consistent with the previous study (Figure 1). The BEAST analysis converged after 1.9 x 10^8 generations, except for a few parameters associated with the Birth-Death Model (see Claramunt and Cracraft, 2015), which had Effective Sample Size values slightly below 200. The analysis recovered a crown age of 53.65 (95% HPD = 49.18–58.02) mya for crown Passeriformes, 49.89 (95% HPD = 45.81–53.83) mya for stem Tyranni, 42.53 (95% HPD = 37.72–47.46) for crown Tyrannides-Furnariides, 38.75 (95% HPD = 27.44–39.5) mya for crown Tyrannides, and 26.14 (95% HPD = 19.75–32.66) mya for crown Tityridae, which were used as secondary node calibrations for the MCMCTree analysis. The BEAST phylogeny additionally recovered ages of 17.11 (95% HPD = 9.98–24.25) mya for the split between *Xenopsaris* and *Pachyramphus* (stem *Pachyramphus*), 14.76 (95% HPD = 7.68–22.1) mya for crown *Pachyramphus*, 19.97 (95% HPD = 12.81–26.91) for the split between *Tityra* and *Xenopsaris+Pachyramphus* (stem *Tityra*).

The results of our MCMCTree on filtered UCE loci converged, with all ages and parameter values that showed high ESS values above 500. We recovered an age of 22.9 (95% HPD = 18.80–26.27) mya for the crown split of Tityrinae, 8.53 (95% HPD = 5.33–12.33) mya for *Tityra*, 11.68 (95% CI = 8.84–14.88) mya for crown *Pachyramphus*, and 2.51 (95% HPD = 0.58–6.01) mya for crown *Iodopleura.* The split between *Xenopsaris* and *Pachyramphus* was recovered to be 13.44 (95% HPD = 10.29–16.89) mya (Figure 1). Higher-taxon ages from each tree and from an additional study (Prum et al., 2015) are summarized in Table S2.

Macroevolutionary rates

TESS analyses of episodic diversification found a trend of increasing speciation and decreasing extinction rates through time (Figure S3). In BAMM, the best shift configuration (maximum posterior probability of rates through time) found increasing speciation and net-diversification rates through time, and constant extinction rates through time (Figure S3). Our best model in DDD was a model without carrying capacity (AICc = 222.151, AICω = 0.354), but this model was only a marginal improvement over the five other models (AICω = 0.106–0.237). Four of these models, however, estimated values of K ranging from ~190,000 to infinity. The final model estimated K to be nearly 2000. Taken together these results suggest that there is no meaningful effect of K on net-diversification rates.

We additionally found a relationship between palaeotemperature and net-diversification rates (slope = -0.03279± 0.003222, intercept = 0.2735 ± 0.02143, $p < 10^{-15}$; Adjusted R-squared = 0.6833, F = 103.6. df = 48, $p < 10^{-12}$). The best-fitting glm was one where net-diversification varies as a function of interactive effects of time and temperature (Table S4). Model selection in RPANDA, however, showed that a model where speciation rate varies exponentially with time (AICc = 231.9682, AICω = 0.2660) is marginally better-fitting than a model where speciation rate varies exponentially with temperature (AICc = 232.3937, AICω = 0.2151), though the difference in AICω was not significant (Table S5). Estimates of α (exponential scaler for speciation rate) were negative for all RPANDA models indicating that speciation rate increases with decreasing temperature and with decreasing time before present.

Supplementary Discussion

A novel method for filtering of sequence capture data

We designed a novel model-based framework for identifying aberrant loci to remove from high-throughput sequencing datasets. Large molecular datasets, such as those resulting from sequence capture approaches, can be highly variable in locus informativeness and utility. While most modern techniques for estimating phylogeny and divergence times are robust to genetree discordances due to incomplete lineage sorting, deep coalescence, and (sometimes) hybridization, gene tree error can be a major source of noise and bias in molecular datasets (Richards et al., 2018). Similarly, high throughput datasets can be very difficult to analyze due to their size and analyzing these data is often intractable over reasonable time frames (Smith et al., 2018). Thus, filtering and subsampling data are often necessary steps for improving efficiency of analyses.

Our filtering protocol follows previous studies' attempts to quantify both informativeness and clock-likeness of molecular markers based on parsimony informative sites and likelihood ratios, respectively (Doyle et al., 2015; Manthey et al., 2016). We evaluated these metrics for our molecular dataset and found that informativeness and clock-likeness were correlated. We used this information to model LR as a function of informativeness and identified those loci which were most influential in the model, under the assumption that those loci could be a source of noise. Those loci contained primarily very un-clocklike genes, though a handful of genes were more clocklike, including two which were among the most clocklike markers in the dataset (Figure S1). Thus, identifying outliers was worthwhile, even though we only chose to use the 15 most clocklike markers in the filtered dataset. Had we not identified outliers first, some of the markers may have biased our results. More work is needed in order to evaluate the efficacy of this protocol in comparison to, for example, randomly sampling markers.

Macroevolutionary rates

Virtually all models estimated parameters that were consistent with positive net-diversification rates and thus increasing diversity through time (Figures 3, S3, S4, S5, and S6). Only TESS estimated negative net-diversification rates early in Tityrinae's history, but this result is contrary to the bulk of macroevolutionary modeling results. Although BAMM also showed an overall increase in rates of net-diversification over time, speciation rate was always higher than extinction rate. Similarly, all models in DDD estimated speciation rates to be greater than extinction rates, thereby supporting the observed pattern of increasing diversity through time, and negative values for α in all of the RPANDA models are also consistent with increasing net-diversification rates toward present (Table S5; Figure S6). Negative α in temperature-dependent models indicates that speciation rates increase with decreasing temperature. Because contemporary temperatures are lower close to the present, this result is consistent with increasing net-diversification at present. Similarly, negative estimates for α in time-dependent models show that speciation rate increases with decreasing time before the present. Therefore, speciation rates are highest at time = 0 (present) and lowest at time = ~23 (Tityrinae origin).

The best-fitting DDD model was one where K was not estimated, thereby rejecting models of diversity-dependent diversification. Interestingly, models that did incorporate K estimated K to be extremely high (Table S3). For example, all DDD models except one estimated K to be at least one order of magnitude higher than the total number of extant bird species (10,000–20,000 avian species in total; e.g., Barrowclough et al., 2016) and thus four orders of magnitude higher than all extant Tityrinae. Even the model with the lowest estimate of

K (the third-best model) estimates K to be nearly 2000 species. These abnormally high estimates indicate that K has no effect on net-diversification and that diversity-dependent mechanisms have had no influence on Tityrinae diversification.

We also statistically evaluated the effect of temperature on net-diversification. Although we find a strong negative relationship between palaeotemperature and net-diversification rates (Figures 3, S5, and S6), we lacked robust statistical support to show that temperature alone explains diversification rates better than time (Table S5; Figure S6). For example, although temperature explains nearly 68% of the variance in net-diversification rates through time estimated in TESS, time explains roughly 94%. Our best-fitting glm, on the other hand, was a model where net-diversification varies with interactions of time and temperature. That is, under the best glm, net-diversification varies with time, but the effect of time on net-diversification also varies with temperature. Therefore, based on the glms, time and temperature are both important parameters influencing diversification.

As an independent test of climate-mediated diversification, RPANDA resulted in statistical uncertainty. When conditioning on stem ages we showed that a model where speciation rate varied as a function of palaeotemperature was nearly as well-fitting as a model where rates only varied with time, and we find similar results when conditioning on the crown ages. Here, time may be the most important predictor of net-diversification rate, but this observation is still consistent with a hypothesis of barrier displacement if the rate of barrier formation and degradation is relatively constant through time (e.g., see Albert et al., 2017). While palaeotemperature has likely played some role in influencing barrier displacement, temperature is just one parameter out of a large number of variables that may influence barrier change. For example, additional unmeasured factors such as precipitation, erosion, and tectonics are also important parameters in a model of barrier displacement, but would be difficult (if not impossible) to measure and factor into our analyses.

We also suspect that imprecise estimates of divergence times in our dated phylogeny could bias the RPANDA results and limit the fit of the models to the data, and that our dataset lacks the power to distinguish among models due to relatively small sample size. For example, it would be very difficult to measure slight increases and decreases in speciation rate over relatively short periods on the order of 10^4 years based on a tree with 50 terminal taxa with posterior densities of node ages in the order of 10^6 years (Figure 1). However, that same time frame of 10^4 years is the temporal scale in which we see many dramatic shifts in global temperature. Therefore, levels of temporal precision in the temperature dataset are far finer and more exact than levels of precision in our divergence times and subsequent net-diversification rate estimates. The problems of sample size and precision are also reflected in the wide posterior densities surrounding parameter estimates in TESS (Figures 3 and S3). Furthermore, on a spatial scale, temperature is likely imprecise because we use global measurements, which do not pick up local effects driven by, for example, Andean orogenic uplift.

Because of temporal imprecision, net-diversification rate estimates probably become somewhat smoothed through time. We attempted to circumvent the problem of disparate degrees of temporal precision by "smoothing" temperature measurements. To do this, we took mean temperatures during ~450,000-year intervals (Table S4). By averaging temperatures over longer periods of time, we reduce the temporal precision of the temperature dataset, thereby improving comparability of the two datasets (i.e., diversification rates and temperature). Remarkably, this resulted in a statistically significant result that showed that a model where net-diversification rate

varies in relation to interactions of time and temperature greatly outperforms the other models where net-diversification rate varies in relation to time or temperature alone (Table S4).

Nevertheless, more data are needed in order to more robustly determine the relationship between temperature and diversification. Even though we lack a robust causal relationship between temperature and net-diversification rate, we suggest that future studies should further investigate this relationship in detail. Specifically, studies that sample large clades (hundreds or thousands of species) at dense taxonomic scales (e.g., subspecies, phylogenetic species, or "coalescent" species) and use rigorous fossil-calibrated divergence dating based on genome-wide markers may provide increased precision of divergence times and rates of diversification through time. Additionally, modeling diversification as a function of climate at more local scales (i.e., South American instead of global) and including measures of precipitation, if possible, might assist in teasing apart the relative effects of time and palaeoclimate.

Diversification in Amazonia

Amazonia is known for its high species richness and debates over how this diversity was generated have been ongoing for decades (Haffer, 1969; Cracraft and Prum, 1988; Smith et al., 2014). All early divergences within Tityrinae appear to have occurred within proto-Amazonia but are not easily-explained by the presence of current barriers that separate extant clades. This is probably due the dynamic history of those barriers through landscape changes over the last ten million years. For example, the Aripuanã River, which was likely an important historical barrier, has since become a less effective dispersal barrier (Fernandes et al., 2012, 2014; Ferreira et al., 2017). Within-Amazonian splits were clearly important for generating diversity in Tityrinae from the Miocene through the Pleistocene, as *in situ* speciation in Amazonia was exceptionally high (Figure 2). Although the timing of the establishment of the Amazon River drainage is still debated (Campbell et al., 2006; Hoorn et al., 2010; Nogueira et al., 2013), the existence of a massive mega-wetland system, called Pebas, in western Amazonia during the Miocene is well-known based on fossil vertebrates, palynology, and sedimentology (Latrubesse, et al., 2010; Antoine et al., 2015; Salas-Gismondi et al., 2015; Tejada-Lara et al., 2015). Similarly, Miocene Amazonia saw a series of marine transgressions that may have separated populations of organisms in the Andean foothills, Guiana Shield, and Brazilian Shield (Aleixo and Rossetti, 2007). Transgressions are thought to have occurred at roughly 15-13 mya and possibly again at 10-5 mya (Hernandez et al., 2005; Aguilera et al., 2013; Jaramillo et al., 2017), which roughly corresponds to early splits in Tityrinae. In combination with a dynamic fluvial landscape that postdates the Miocene (Campbell et al., 2006; Latrubesse et al., 2010; Hoorn et al., 2010; Ribas et al., 2012), these marine transgressions may have contributed to high *in situ* speciation for Tityrinae in Amazonia (Figure 2).

Atlantic-Amazonian connections

Much variance exists in the timing of speciation between taxon-pairs between Atlantic and Amazonian forests (see main text). For example, splits between *P. m. marginatus* and *P. m. nanus* across this region are likely tied to relatively old Amazon-Atlantic forest connections that existed in the south, while younger splits within *P. polychopterus* in the south may be associated with more recent climatically-mediated gallery and dry forest connections and regressions between southern ecosystems (Arruda et al., 2018; Costa et al., 2018; Trujillo-Arias et al., 2018). Extensive wetlands connecting the western Amazonia and Paraná basins during the Miocene may have facilitated connectivity between river edge specialists and/or gallery forest birds until

the formation of the Fitzcarrald arch roughly 4 Ma (Espurt et al., 2010; Tagliacollo et al., 2015), which may have isolated populations of humid forest and edge taxa from east to west. However, previous work has demonstrated that speciation times across this region vary, rendering the effect of this arch on avian speciation uncertain (Claramunt, 2014). Even so, the relationship between Amazonian river edge specialists (e.g., *P. polychopterus nigriventris*) and southeastern South American taxa (e.g., *P. polychopterus spixii*) documented by a previous study is recapitulated by Tityrinae herein (Claramunt, 2014).

Supplementary Literature Cited:

1. Aguilera, O., Lundberg, J., Birindelli, J., Sabaj Perez, M., Jaramillo, C., Sanchez-Villagra, M.R., 2013. Palaeontological evidence for the last temporal occurrence of the ancient western Amazonian river outflow into the Caribbean. *PloS one* 8, e76202.
2. Albert, J.S., *et al*. 2017. Barrier displacement on a neutral landscape: toward a theory of continental biogeography. *Systematic biology*, *66*(2), 167-182.
3. Aleixo, A., & de Fátima Rossetti, D. 2007. Avian gene trees, landscape evolution, and geology: towards a modern synthesis of Amazonian historical biogeography?. *Journal of Ornithology*, *148*(2), 443-453.
4. Antoine, P.O., Abello, M.A., Adnet, S., Sierra, A.J.A., Baby, P., Billet, G., Boivin, M., Calderón, Y., Candela, A., Chabain, J., Corfu, F., *et al.* 2016. A 60-million-year Cenozoic history of western Amazonian ecosystems in Contamana, eastern Peru. *Gondwana Res* 31, 30-59.
5. Arruda, D.M., *et al.* 2018. Vegetation cover of Brazil in the last 21 ka: New insights into the Amazonian refugia and Pleistocenic arc hypotheses. *Global Ecol Biogeogr* 27, 47-56.
6. Barrowclough, G. F., Cracraft, J., Klicka, J., & Zink, R. M. (2016). How many kinds of birds are there and why does it matter?. *PLoS One*, *11*(11), e0166307.
7. Bouckaert, R., *et al.* 2014. BEAST 2: a software platform for Bayesian evolutionary analysis. *PLoS computational biology*, *10*(4), e1003537.
8. Campbell Jr, K. E., Frailey, C. D., & Romero-Pittman, L. 2006. The Pan-Amazonian Ucayali Peneplain, late Neogene sedimentation in Amazonia, and the birth of the modern Amazon River system. *Palaeogeography, Palaeoclimatology, Palaeoecology*, *239*(1-2), 166-219.
9. Claramunt, S. 2014. Phylogenetic relationships among Synallaxini spinetails (Aves: Furnariidae) reveal a new biogeographic pattern across the Amazon and Paraná river basins. *Molecular phylogenetics and evolution*, *78*, 223-231.
10. Claramunt, S., & Cracraft, J. 2015. A new time tree reveals Earth history's imprint on the evolution of modern birds. *Science Advances*, *1*(11), e1501005.
11. Condamine *et al.* 2013. Macroevolutionary perspectives to environmental change. *Ecology letters*, *16*, pp.72-85.
12. Costa, G.C., *et al.* 2018. Biome stability in South America over the last 30 kyr: Inferences from long-term vegetation dynamics and habitat modelling. *Global Ecol Biogeogr* 27, 285-297.
13. Cracraft, J. & Prum, R.O. 1988. Patterns and processes of diversification: speciation and historical congruence in some Neotropical birds. *Evolution*, *42*(3), 603-620.
14. Doyle, V. P., Young, R. E., Naylor, G. J., & Brown, J. M. 2015. Can we identify genes with increased phylogenetic reliability?. *Systematic biology*, *64*(5), 824-837.

15. Espurt, N., *et al.* 2010. The Nazca Ridge and uplift of the Fitzcarrald Arch: implications for regional geology in northern South America. *Amazonia, Landscape and Species Evolution: A Look into the Past. Blackwell-Wiley*, 89-100.
16. Etienne, R. S., Haegeman, B., Stadler, T., Aze, T., Pearson, P. N., Purvis, A., & Phillimore, A. B. (2011). Diversity-dependence brings molecular phylogenies closer to agreement with the fossil record. *Proc. R. Soc. B*, rspb20111439.
17. Faircloth, B. C., *et al.* 2012. Ultraconserved elements anchor thousands of genetic markers spanning multiple evolutionary timescales. *Systematic biology*, *61*(5), 717-726.
18. Fernandes, A. M., Wink, M., & Aleixo, A. 2012. Phylogeography of the chestnut-tailed antbird (Myrmeciza hemimelaena) clarifies the role of rivers in Amazonian biogeography. *Journal of Biogeography*, *39*(8), 1524-1535.
19. Fernandes, A. M., Wink, M., Sardelli, C. H., & Aleixo, A. 2014. Multiple speciation across the A ndes and throughout A mazonia: the case of the spot-backed antbird species complex (Hylophylax naevius/Hylophylax naevioides). *Journal of biogeography*, *41*(6), 1094-1104.
20. Ferreira, M., Aleixo, A., Ribas, C. C., & Santos, M. P. D. 2017. Biogeography of the Neotropical genus Malacoptila (Aves: Bucconidae): the influence of the Andean orogeny, Amazonian drainage evolution and palaeoclimate. *Journal of biogeography*, *44*(4), 748-759.
21. Fitzpatrick, J. W., del Hoyo, J., Elliot, A., & Christie, D. A. 2004. Handbook of the birds of the world. Vol. 9. Cotingas to pipits and wagtails. *Handbook of the birds of the world Vol. 9, Cotingas to pipits and wagtails*.
22. Haffer, J. 1969. Speciation in Amazonian forest birds. *Science*, *165*(3889), 131-137.
23. Hernández, R. M., Jordan, T. E., Farjat, A. D., Echavarría, L., Idleman, B. D., & Reynolds, J. H. (2005). Age, distribution, tectonics, and eustatic controls of the Paranense and Caribbean marine transgressions in southern Bolivia and Argentina. *Journal of South American Earth Sciences*, *19*(4), 495-512.
24. Höhna, S., *et al.* 2016. RevBayes: Bayesian phylogenetic inference using graphical models and an interactive model-specification language. *Systematic Biology*, *65*(4), 726-736.
25. Höhna, S., *et al.* 2016. TESS: an R package for efficiently simulating phylogenetic trees and performing Bayesian inference of lineage diversification rates. *Bioinformatics*, *32*(5), 789-791.
26. Hosner, P. A., Faircloth, B. C., Glenn, T. C., Braun, E. L., & Kimball, R. T. 2015. Avoiding missing data biases in phylogenomic inference: an empirical study in the landfowl (Aves: Galliformes). *Molecular Biology and Evolution*, *33*(4), 1110-1125.
27. Jaramillo, C., Klaus, S., Marivaux, L., Navarrete, R.E., Orliac, M.J., Parra, F., Pérez, M.E., Pujos, F., Rage, J.-C., Ravel, A., Robinet, C., *et al.* 2016. A 60-million-year Cenozoic history of western Amazonian ecosystems in Contamana, eastern Peru. *Gondwana Res* 31, 30-59.
28. Jarvis, E. D., Mirarab, S., Aberer, A. J., Li, B., Houde, P., Li, C., *et al*. 2014. Whole-genome analyses resolve early branches in the tree of life of modern birds. *Science*, *346*(6215), 1320-1331.
29. Katoh K, Standley DM. 2013. MAFFT multiple sequence alignment software version 7: improvements in performance and usability. *Molecular biology and evolution 30*(4):772-80.

30. Latrubesse, E.M., *et al.* 2010. The Late Miocene paleogeography of the Amazon Basin and the evolution of the Amazon River system. *Earth-Science Reviews*, *99*(3-4), 99-124.
31. Manthey, J. D., Campillo, L. C., Burns, K. J., & Moyle, R. G. 2016. Comparison of target-capture and restriction-site associated DNA sequencing for phylogenomics: a test in cardinalid tanagers (Aves, Genus: Piranga). *Systematic biology*, *65*(4), 640-650.
32. Matzke, N. J. 2013. BioGeoBEARS: biogeography with Bayesian (and likelihood) evolutionary analysis in R scripts. *R package, version 0.2*, *1*, 2013.
33. Morlon, H., *et al.* 2016. RPANDA: an R package for macroevolutionary analyses on phylogenetic trees. *Methods in Ecology and Evolution*, *7*(5), 589-597.
34. Musher, L. J., & Cracraft, J. 2018. Phylogenomics and species delimitation of a complex radiation of Neotropical suboscine birds (Pachyramphus). *Molecular phylogenetics and evolution*, *118*, 204-221.
35. Nogueira, A.C.R., Silveira, R., Guimarães, J.T.F., 2013. Neogene–Quaternary sedimentary and paleovegetation history of the eastern Solimões Basin, central Amazon region. *Journal of South American Earth Sciences* 46, 89-99.
36. Paradis, E., Claude, J. and Strimmer, K. 2004. APE: analyses of phylogenetics and evolution in R language. Bioinformatics, 20, 289–290.
37. Parker, T., Stotz, D., & Fitzpatrick, J. 1996. Database A: zoogeography and ecological attributes of bird species breeding in the Neotropics. *Neotropical birds: ecology and conservation.* University of Chicago Press, Chicago, 131-291.
38. Prum, R.O., Berv, J.S., Dornburg, A., Field, D.J., Townsend, J.P., Lemmon, E.M. and Lemmon, A.R., 2015. A comprehensive phylogeny of birds (Aves) using targeted next-generation DNA sequencing. *Nature*, *526*(7574), p.569.
39. Rabosky, D. L., *et al.* 2014. BAMMtools: an R package for the analysis of evolutionary dynamics on phylogenetic trees. *Methods in Ecology and Evolution*, *5*(7), 701-707.
40. Rambaut, A., Suchard, M. A., Xie, D., & Drummond, A. J. (2014). Tracer v1. 6. available from http. *beast. bio. ed. ac. uk/Tracer*.
41. Ree, R. H., & Smith, S. A. 2008. Maximum likelihood inference of geographic range evolution by dispersal, local extinction, and cladogenesis. *Syst. Biol.*, *57*(1), 4-14.
42. Revell, L. J. 2012. phytools: an R package for phylogenetic comparative biology (and other things). *Methods in Ecology and Evolution*, *3*(2), 217-223.
43. Ribas, C.C., *et al.* 2007. The assembly of montane biotas: linking Andean tectonics and climatic oscillations to independent regimes of diversification in Pionus parrots. *Proc. R. Soc. B*, *274*(1624), 2399-2408.
44. Richards, *et al.* 2018. Variation across mitochondrial gene trees provides evidence for systematic error: How much gene tree variation is biological?. *Systematic biology*, 67(5), 847–860.
45. Salas-Gismondi, R., Flynn, J. J., Baby, P., Tejada-Lara, J. V., Wesselingh, F. P., & Antoine, P. O. 2015. A Miocene hyperdiverse crocodylian community reveals peculiar trophic dynamics in proto-Amazonian mega-wetlands. *Proceedings of the Royal Society of London B: Biological Sciences*, *282*(1804), 20142490.
46. Silvestro, D., & Michalak, I. 2012. raxmlGUI: a graphical front-end for RAxML. *Organisms Diversity & Evolution*, *12*(4), 335-337.
47. Smith, B.T., *et al.* 2014. The drivers of tropical speciation. *Nature*, *515*(7527), 406.
48. Stamatakis A. 2006. RAxML-VI-HPC: maximum likelihood-based phylogenetic analyses with thousands of taxa and mixed models. *Bioinformatics*. 22(21):2688-90.

49. Tagliacollo, V.A., *et al.* 2015. Biogeographical signature of river capture events in Amazonian lowlands. *Journal of biogeography*, *42*(12), 2349-2362.
50. Tejada-Lara, J. V., Salas-Gismondi, R., Pujos, F., Baby, P., Benammi, M., Brusset, *et al.* 2015. Life in proto-Amazonia: Middle Miocene mammals from the Fitzcarrald Arch (Peruvian Amazonia). *Palaeontology*, *58*(2), 341-378.
51. Tello, J. G., Moyle, R. G., Marchese, D. J., & Cracraft, J. 2009. Phylogeny and phylogenetic classification of the tyrant flycatchers, cotingas, manakins, and their allies (Aves: Tyrannides). *Cladistics*, *25*(5), 429-467.
52. Trujillo-Arias, N., *et al.* 2018. Forest corridors between the central Andes and the southern Atlantic Forest enabled dispersal and peripatric diversification without niche divergence in a passerine. *Molecular phylogenetics and evolution*, *128*, 221-232.
53. Zerbino D, Birney E. 2008. Velvet: algorithms for de novo short read assembly using de Bruijn graphs. *Genome research*. 074492.

Supplementary Tables:

Table S1: A list of all samples used in this study.

Material	Institution	Tissue/Coll. #	Genus	Species	Subspecies	Coded_as	Citation
Tissue	Cantebury Museum		*Acanthisitta*	*chloris*		acachl	Jarvis et al., 2014
Tissue	AMNH	DOT 12145	*Elaenia*	*albiceps*	*chilensis*	Elaenia_albiceps_chilensis_DOT12145	This study
Tissue	USNM	626253	*Iodopleura*	*fusca*		Iodop_fusca_S626253	NSF grant 1146248
Tissue	LSUMNS	9597	*Iodopleura*	*isabellae*		Iodop_isalae_L9597	NSF grant 1146248
Tissue	MPEG	55056	*Lepidothrix*	*nattereri*		Lep_nat_MPEG55056	This study
Tissue	FMNH	393859	*Pachyramphus*	*aglaiae*	*albiventris*	P_a_alb393859	Musher and Cracraft, 2018
FJ501700.1	AMNH	3688	*Pachyramphus*	*aglaiae*	*latirostris*	Pachyramphus_agliae1 [RAG dataset]	Tello et al., 2009
Tissue	UWBM	104042	*Pachyramphus*	*aglaiae*	*sumichrasti*	Pac_sum104042	Musher and Cracraft, 2018
Skin	AMNH	494147	*Pachyramphus*	*albogriseus*	*albogriseus*	P_albogriseus_494147	This study
Tissue	LSUMNS	33450	*Pachyramphus*	*albogriseus*	*guayaquilensis*	P_a_gua33450	Musher and Cracraft, 2018
Tissue	LSUMNS	41620	*Pachyramphus*	*albogriseus*	*ornatus*	P_a_orn_41620	Musher and Cracraft, 2018
Tissue	LSUMNS	8114	*Pachyramphus*	*albogriseus*	*salvini*	Pac_salv8114	Musher and Cracraft, 2018
Tissue	FMNH	390007	*Pachyramphus*	*castaneus*	*amazonus*	P_c_ama390007	Musher and Cracraft, 2018
Tissue	FMNH	395729	*Pachyramphus*	*castaneus*	*castaneus*	P_c_cas395729	Musher and Cracraft, 2018
Tissue	LSUMNS	46602	*Pachyramphus*	*cinnamomeus*	*cinnamomeus*	P_c_cin46602	Musher and Cracraft, 2018
Tissue	LSUMNS	8812	*Pachyramphus*	*cinnamomeus*	*fulvidior*	P_c_fulv8812	Musher and Cracraft, 2018
Tissue	LSUMNS	12174	*Pachyramphus*	*homochrous*	*homochrous*	P_h_hom12174	Musher and Cracraft, 2018
Tissue	LSUMNS	2306	*Pachyramphus*	*homochrous*	*homochrous*	P_h_hom2306	Musher and Cracraft, 2018
Tissue	UAM	KSW 1195	*Pachyramphus*	*major*	*itzensis*	P_tzensis_1195	This study
Tissue	UWBM	101156	*Pachyramphus*	*major*	*uropygialis*	P_m_uro101156	Musher and Cracraft, 2018
Tissue	MPEG	UNA 141	*Pachyramphus*	*marginatus*	*marginatus*	P_marginatus_141	This study
Tissue	LSUMNS	7221	*Pachyramphus*	*marginatus*	*nanus*	P_nanus_7221	Musher and Cracraft, 2018
Tissue	INPA	5436	*Pachyramphus*	*marginatus*	*nanus*	Pac_nan5436	This study
Tissue	USNM	650772	*Pachyramphus*	*marginatus*	*nanus*	Pac_nan650772	Musher and Cracraft, 2018
Tissue	INPA	13868	*Pachyramphus*	*minor*		Pac_min13868	Musher and Cracraft, 2018
Skin	FMNH	282130	*Pachyramphus*	*polychopterus*	*dorsalis*	Pac_dor282130	Musher and Cracraft, 2018
Tissue	FMNH	473791	*Pachyramphus*	*polychopterus*	*nigriventris*	P_p_nig473791	Musher and Cracraft, 2018
Tissue	FMNH	392915	*Pachyramphus*	*polychopterus*	*polychopterus*	P_p_pol392915	Musher and Cracraft, 2018
Tissue	LSUMNS	60813	*Pachyramphus*	*polychopterus*	*similis*	P_p_sim60813	Musher and Cracraft, 2018
Tissue	FMNH	433661	*Pachyramphus*	*polychopterus*	*spixii*	P_p_spi433661	Musher and Cracraft, 2018
Tissue	USNM	636057	*Pachyramphus*	*polychopterus*	*spixii*	P_spixii_636057	This study
FJ501699.1	AMNH	2286	*Pachyramphus*	*polychopterus*	*spixii*	P_Pachyramphus_polychopterus1 [RAG]	Tello et al., 2009
Tissue	LSUMNS	7299	*Pachyramphus*	*rufus*	*juruanus*	P_r_juru7299	Musher and Cracraft, 2018
Tissue	USNM	643957	*Pachyramphus*	*spodiurus*		P_spod28466	Musher and Cracraft, 2018
Tissue	KU	89835	*Pachyramphus*	*surinamus*		Pac_nan650777 [incorrectly coded]	Musher and Cracraft, 2018
Tissue	AMNH	DOT6128	*Pachyramphus*	*validus*	*audax*	P_v_aud6128	Musher and Cracraft, 2018
Tissue	FMNH	392917	*Pachyramphus*	*validus*	*validus*	P_v_val392917	Musher and Cracraft, 2018
Tissue	LSUMNS	19903	*Pachyramphus*	*versicolor*	*costaricensis*	P_v_cos19903	Musher and Cracraft, 2018
Tissue	LSUMNS	1674	*Pachyramphus*	*versicolor*	*meridionalis*	P_v_meri1674	Musher and Cracraft, 2018
Tissue	IAvH-BT	1630	*Pachyramphus*	*versicolor*	*versicolor*	P_v_vers_1630	Musher and Cracraft, 2018
Tissue	LSUMNS	37974	*Pachyramphus*	*viridis*	*viridis*	P_v_vir37974	Musher and Cracraft, 2018
Tissue	KU	18786	*Pachyramphus*	*xanthogenys*	*peruanus*	P_x_xant_18786	Musher and Cracraft, 2018
FJ501743.1	AMNH	11874	*Schiffornis*	*turdina*		Schiffornis_turdina1 [RAG]	Tello et al., 2009
Tissue	AMNH	DOT2451	*Schiffornis*	*virescens*		Schiffornis_virescens_DOT2451	This study
Tissue	AMNH	DOT12143	*Scytalopus*	*fuscus*		Scytalopus_fuscus_DOT12143	This study
Tissue	MPEG	GDL 023	*Tityra*	*cayana*	*braziliensis*	Tityra_cayana_GDL_023	This study
Tissue	LSUMNS	3145	*Tityra*	*cayana*	*cayana*	Tityra_cayan_L3145	This study
Skin	FMNH	282133	*Tityra*	*inquisitor*	*buckleyi*	Tityra_inquisitor_buckleyi_FMNH_282133	This study
Tissue	KU	3625	*Tityra*	*inquisitor*	*inquisitor*	Tityra_inquis_KU3625	NSF grant 1146248
Tissue	MPEG	UFAC 422	*Tityra*	*inquisitor*	*pelzelni*	Tityra_inquisitor_UFAC_422	This study
Skin	AMNH	408024	*Tityra*	*semifasciata*	*columbiana*	Tityra_columbiana_408024	This study
Tissue	AMNH	DOT3682	*Tityra*	*semifasciata*	*costaricensis*	Tit_sem3682	This study
Skin	AMNH	493766	*Tityra*	*semifasciata*	*deses*	Tityra_deses_493766	This study
Tissue	FMNH	474321	*Tityra*	*semifasciata*	*fortis*	Tityra_semata_474321	This study
Tissue	MPEG	ORX425	*Tityra*	*semifasciata*	*semifasciata*	Tityra_semata_MPEGORX425	This study
Tissue	MPEG	AMZ 082	*Troglodytes*	*musculus*		Tr_musculus	Tiago Souza (MPEG)
Tissue	ANSP	8359	*Xenopsaris*	*albinucha*		X_albin627351	Musher and Cracraft, 2018
FJ501767.1	ANSP	8359	*Xenopsaris*	*albinucha*		Xenopsaris_albinucha [RAG]	Tello et al., 2009

Table S2: Age estimates for a set of clades based on our analyses in addition to a recently published phylogenomic study (Prum et al., 2015).

Dataset/citation	Crown Passeriformes (mya)	Stem Tyranni (mya)	Crown Tyrannides-Furnariides (mya)	Crown Tyrannides (mya)	Crown Tityridae (mya)
RAG (BEAST)	53.8 (49.65–57.82)	50.05 (46.47–53.60)	45.77 (37.88–47.24)	34.33 (28.86–40.59)	26.31 (19.67–33.64)
UCEs 95% (MCMCTree)	55.49 (50.74–58.10)	49.42 (46.38–53.33)	41.51 (37.97–46.16)	29.55 (27.97–32.34)	25.34 (21.35–27.82)
Prum et al., 2015	49 (41.5–55.5)	46.8 (38-53)	38.2 (27–46)	27 (17.5–36.5)	16 (5-25)

Table S3: Model fitting results for diversification models that explicitly incorporate carrying capacity (K) (Etienne et al., 2012). The best-fitting model is shown in bold.

Model	estimated parameters	logL	AICc	AICω	Speciation rate (λ)	Extinction rate (μ)	Carrying Capacity (K)
Birth-death constant rates	**2**	**-108.942**	**222.151**	**0.339**	**0.340**	**0.119**	**NA**
Linear dependence of speciation rate without extinction	2	-109.344	222.954	0.227	0.277	NA	1040588
Linear dependence of speciation rate with extinction	3	-108.942	224.430	0.108	0.340	0.118	189619
Exponential dependence of speciation rate with extinction	3	-109.013	224.572	0.101	0.390	0.149	Infinity
Linear dependence of extinction rate	3	-108.942	224.430	0.108	0.341	0.120	356419
Exponential dependence of extinction rate	3	-108.942	222.151	0.116	0.364	0.087	1742

Table S4: Results for generalized linear model test with averaged values for temperature and net-diversification across 50 intervals during the history of Tityrinae as estimated in TESS. The best model is M3, which models net-diversification rate as a linear function of interactive effects of time and temperature.

Model	Adj. R-squared	slope	standard error	p-value (slope)	intercept	standard error	p-value (intercept)	AIC	AICω
M1: Time	0.943	0.013	0.000	0.000	0.210	0.005	0.000	-243.898	0.009
M2: Temp	0.677	0.274	0.021	0.000	-0.033	0.003	0.000	-157.074	0.000
M3: Time and Temp	0.955	Time 0.009 Temp 0.007 Time:temp 0.001	0.002 0.003 0.000	0.000 0.026 0.027	0.178	0.013	0.000	-253.386	0.991

Table S5: Model-fitting results for ten models: two constant net-diversification, four in which net-diversification varies with time, and four in which net-diversification varies with temperature. Models were conditioned on both stem and crown ages.

Model	Conditioning	Number of parameters	logL	AICc	AICω	speciation rate (λ)	exponential scaler for speciation rate (α)	extinction rate (μ)	exponential scaler for extinction rate (B)
Constant speciation	Stem	1	-116.41	234.90	0.06	0.2501			
Constant speciation and extinction	Stem	2	-114.49	233.24	0.14	0.3865		0.2423	
Speciation varies exponentially with time	Stem	**2**	**-113.85**	**231.97**	**0.26**	**0.3432**	**-0.0706**		
Speciation varies exponentially with time and constant extinction	Stem	3	-113.85	234.24	0.08	0.3432	-0.0706	0.0000	
Extinction varies exponentially with time and constant speciation	Stem	3	-114.21	234.97	0.06	0.3627		0.1633	0.0345
Speciation and extinction vary exponentially with time	Stem	4	-113.85	236.63	0.02	0.3432	-0.0706	0.0000	0.0208
Speciation varies exponentially with temperature	Stem	2	-113.96	232.18	0.23	0.3848	-0.0922		
Speciation varies exponentially with temperature and constant extinction	Stem	3	-113.96	234.46	0.07	0.3846	-0.0922	0.0000	
Extinction varies exponentially with temperature and constant speciation	Stem	3	-114.21	234.97	0.06	0.3627		0.1592	0.0306
Speciation and extinction vary exponentially with temperature	Stem	4	-113.96	236.85	0.02	0.3847	-0.0907	0.0000	0.0250
Constant speciation	crown	1	-115.01	232.11	0.01	0.2452			
Constant speciation and extinction	crown	2	-112.49	229.25	0.06	0.4030		0.2846	
Speciation varies exponentially with time	**crown**	**2**	**-110.91**	**226.09**	**0.28**	**0.3683**	**-0.0962**		
Speciation varies exponentially with time and constant extinction	crown	3	-110.91	228.37	0.09	0.3684	-0.0962	0.0000	
Extinction varies exponentially with time and constant speciation	crown	3	-110.60	227.74	0.12	0.3330		0.0679	0.1361
Speciation and extinction vary exponentially with time	crown	4	-109.54	229.58	0.05	0.3297	-0.0623	0.0003	0.4437
Speciation varies exponentially with temperature	crown	2	-111.43	227.12	0.17	0.4089	-0.1125		
Speciation varies exponentially with temperature and constant extinction	crown	3	-111.36	229.26	0.06	0.4108	-0.0809	0.0666	
Extinction varies exponentially with temperature and constant speciation	crown	3	-110.60	227.74	0.12	0.3330		0.0614	0.1206
Speciation and extinction vary exponentially with temperature	crown	4	110.54	230.01	0.04	0.3505	-0.0594	0.0006	0.3596

Supplementary Figures:

Figure S1: Regressions for clock-likeness (measured by likelihood ratio; LR) as a function of (A) the proportion of informative sites, (B) the number of informative sites, and (C) the log(λ) of per locus, where λ is the optimal smoothing parameter for the penalized likelihood analysis in ape (Paradis et al., 2004). Low values of λ are indicative of higher heterogeneity in branch rates, and thus lower clock-likeness. Gray points represent outlier loci. Gray lines represent each linear model before filtering outliers, and red lines represent the linear model after filtering outliers.

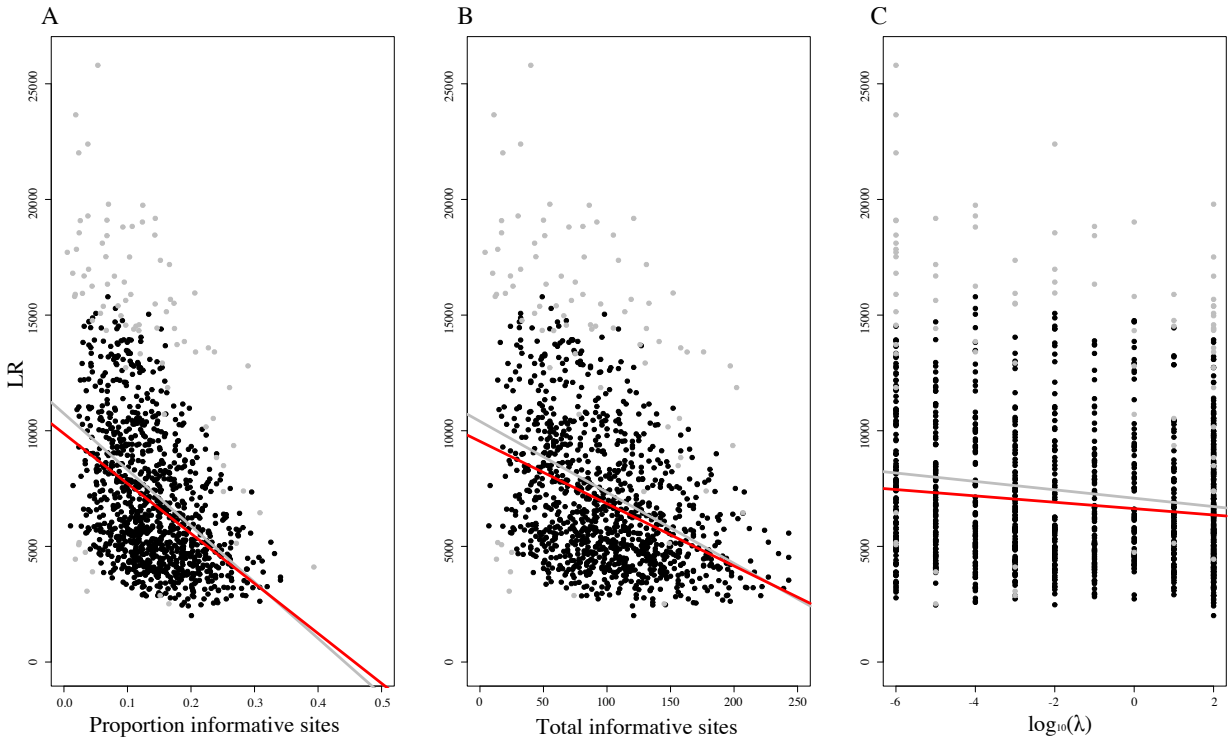

Figure S2: A random subsample of 25 gene trees for loci that were considered outliers and removed from downstream analysis (left), and the 15 most clocklike markers after filtering, which were used for molecular divergence dating analysis (right). The values for number of parsimony informative sites (IS) and the likelihood ratio (LR) are above each gene tree. Values in red represent low LR gene trees that were none-the-less identified as outliers.

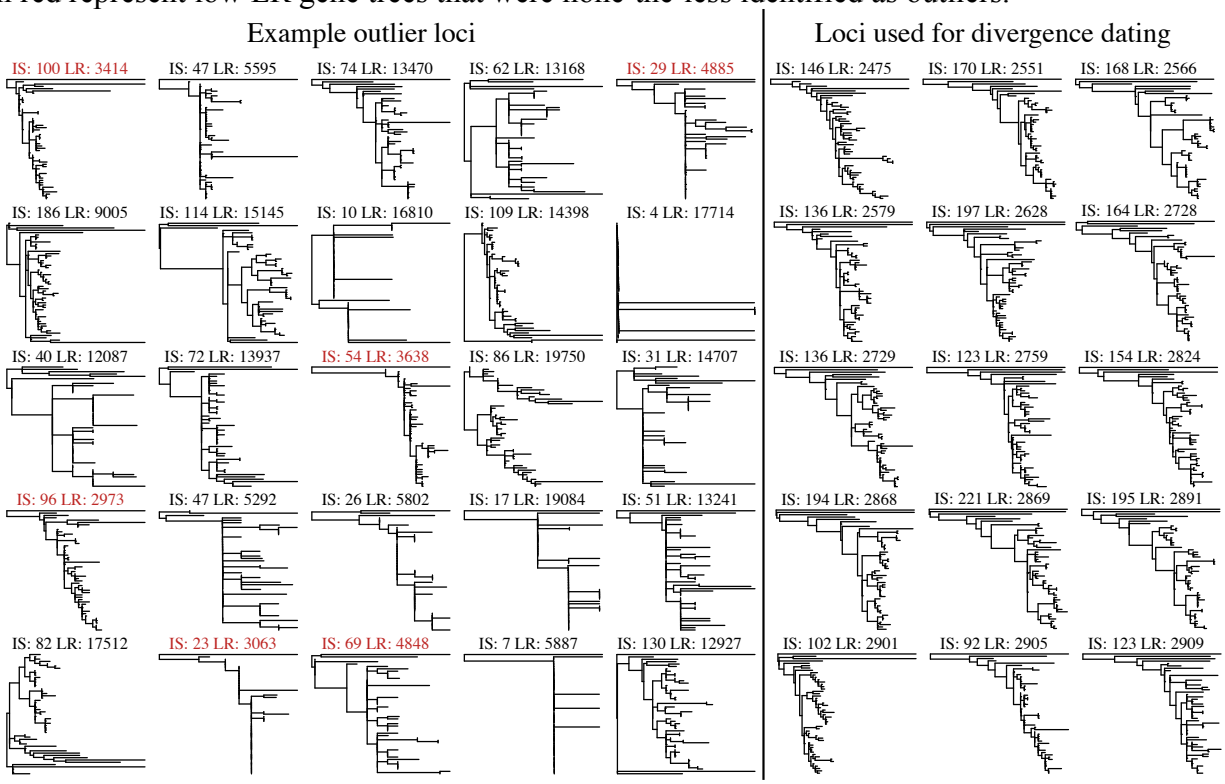

Figure S3: Left: speciation (purple) and extinction (red) rates through time from TESS. Right: The posterior probabilities of speciation (purple bars) and extinction (red bars) rate shifts through time.

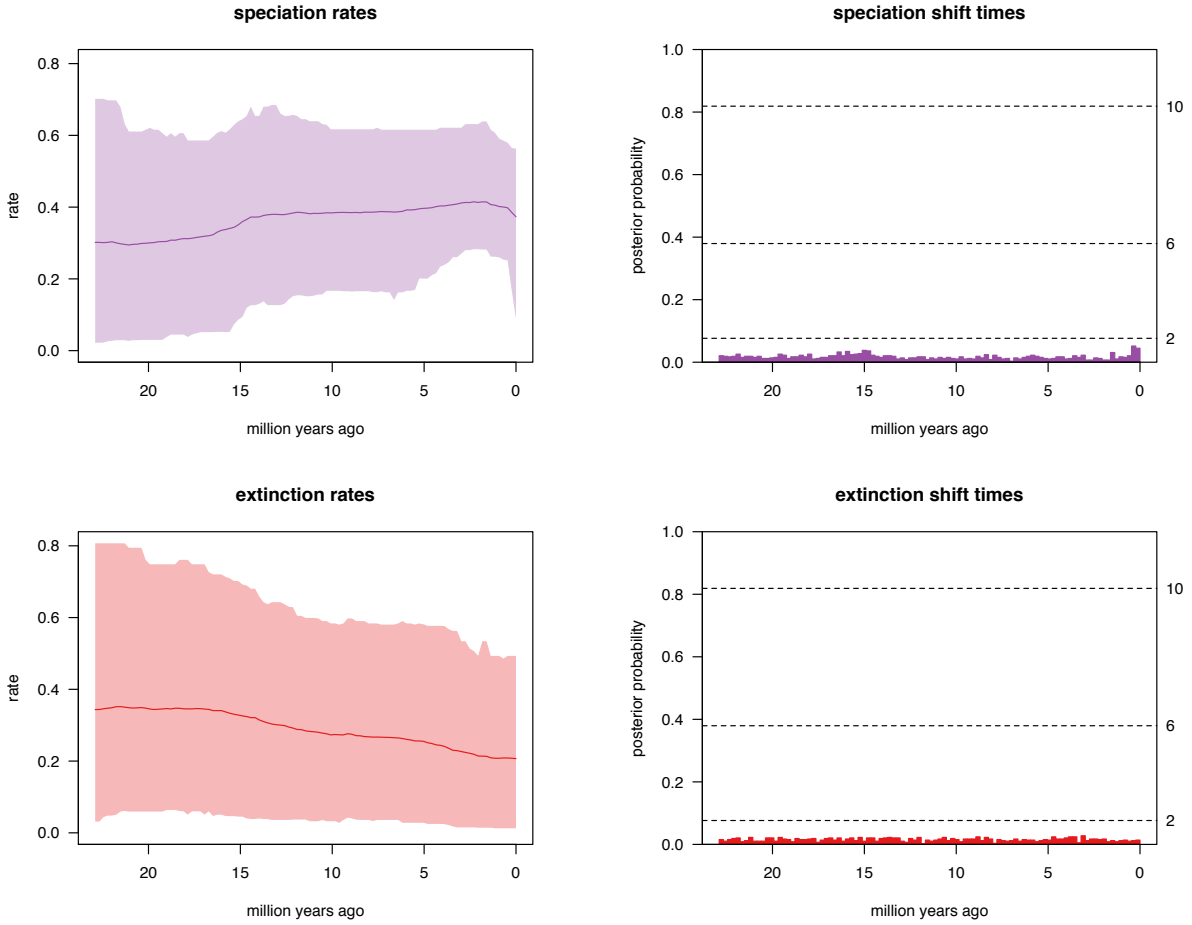

Figure S4: BAMM best shift configuration results for (left to right) speciation rates, extinction rates, and net-diversification rates.

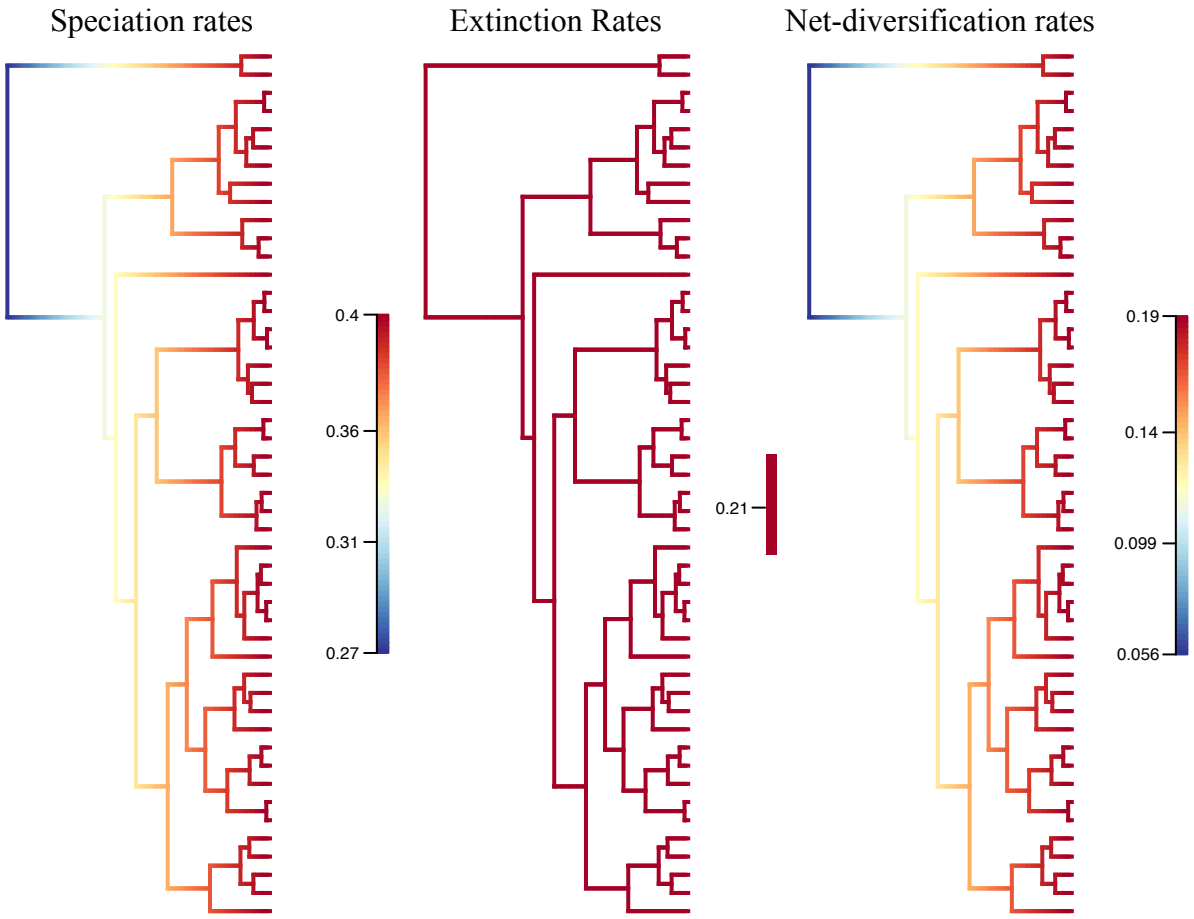

Figure S5: The relationship between net-diversification estimate in TESS and temperature (adj. R-sq. = 0.66813) for 50 intervals between the root and tips of the dated Tityrinae phylogeny.

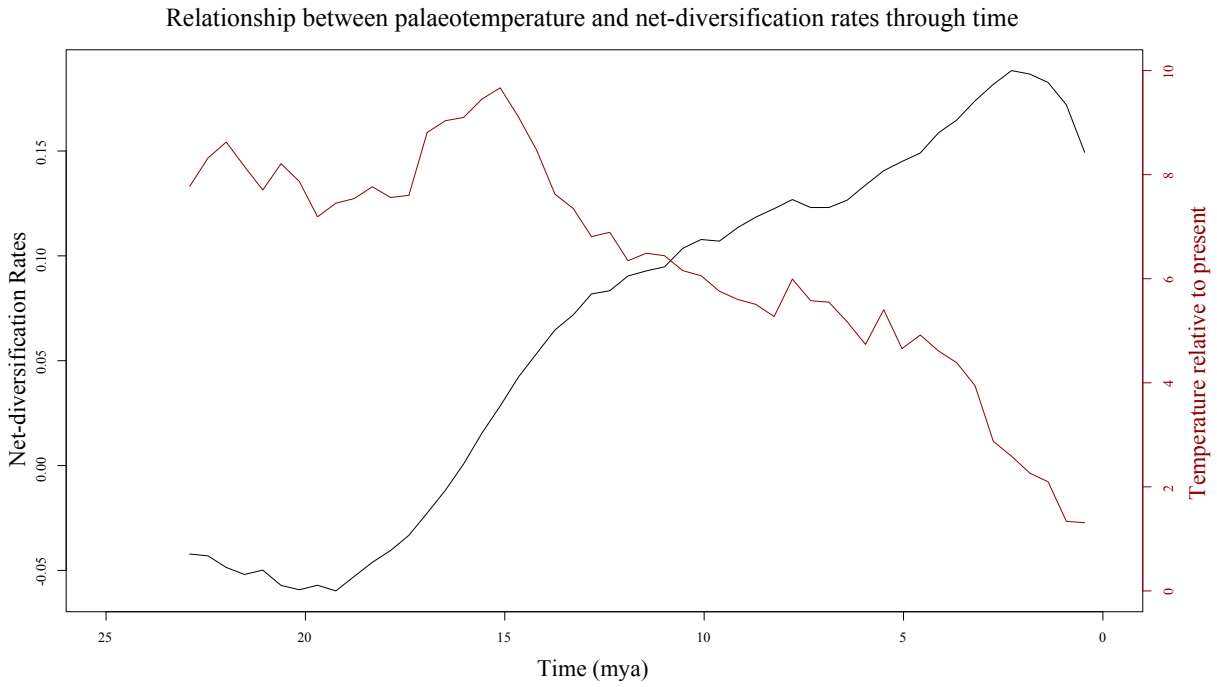

Figure S6: Results from best-fitting RPANDA models conditioned on the crown showing how speciation rate varies as a function of time and palaeoclimate (mean global temperature relative to present). Model-fitted net-diversification estimates for pure birth with exponential dependence on time (top row), and pure birth with exponential dependence on temperature (bottom row).

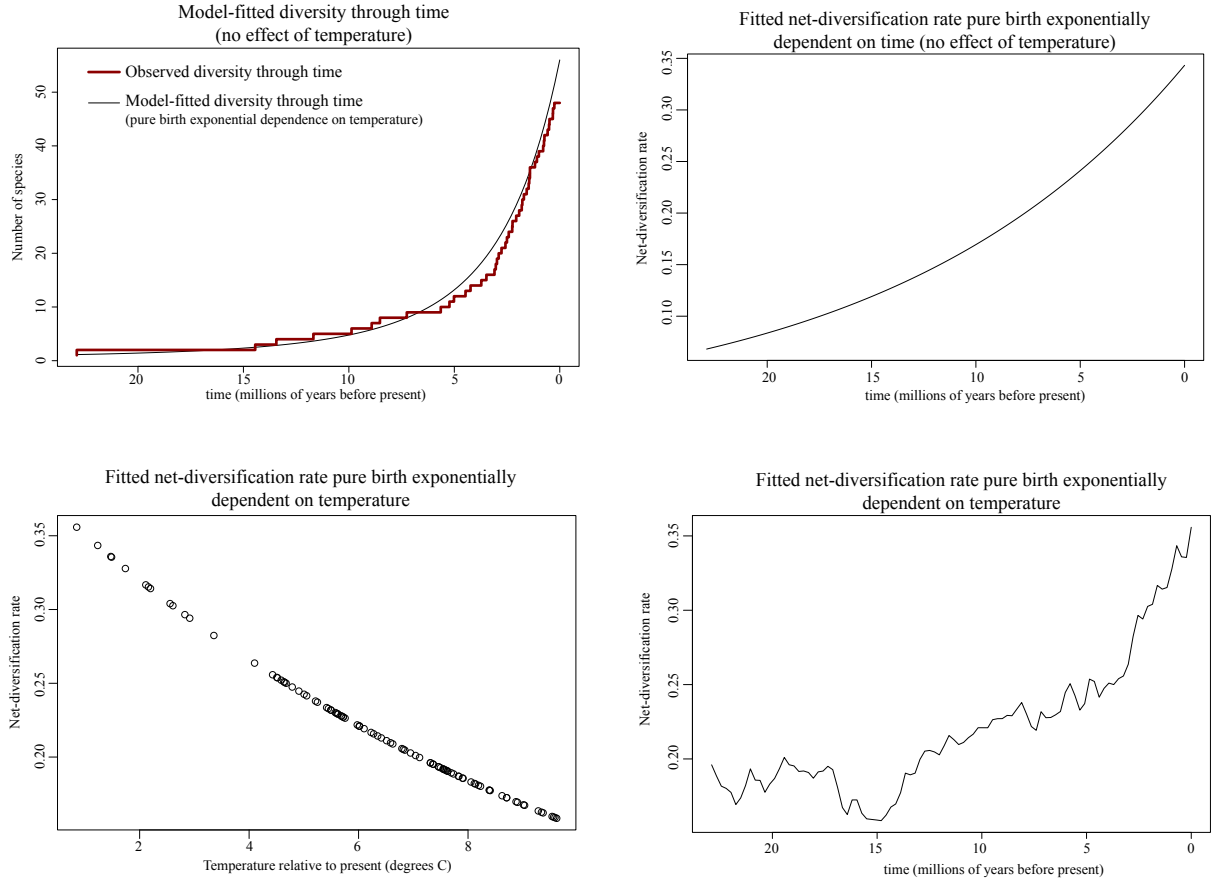

Figure S7: Results from RAxML on concatenated UCEs.